pH-responsive self-assembly of short peptides into multi-catalytic amyloid fibrils

*Marta Díaz-Caballero[1], Susanna Navarro[1], Miquel Nuez-Martínez[2], Francesca Peccati[3], Luis Rodríguez-Santiago[4], Mariona Sodupe[4,5], Francesc Teixidor[2] and Salvador Ventura[1,5]**

[1]Institut de Biotecnologia i de Biomedicina (IBB) and Departament de Bioquímica i Biologia Molecular; Universitat Autònoma de Barcelona; 08193 Bellaterra (Barcelona), Spain.

[2]Institut de Ciència de Materials de Barcelona (ICMAB-CSIC). Campus UAB, 08193 Bellaterra, Barcelona (Spain).

[3]Center for Cooperative Research in Biosciences (CIC bioGUNE), Basque Research and Technology Alliance (BRTA), Bizkaia Technology Park, Building 801A, 48160 Derio (Spain)

[4]Departament de Química, Universitat Autònoma de Barcelona, 08193 Bellaterra (Spain)

[5]ICREA, Passeig Lluís Companys 23, E-08010 Barcelona (Spain)

*Corresponding author: E-mail: salvador.ventura@uab.es

KEYWORDS: amyloid fibrils, self-assembly, short peptides, artificial enzymes, ~~stimuli~~ pH-responsive materials, hydrogels

ABSTRACT

There is an increasing interest in synthetic systems that can execute bio-inspired chemical reactions without requiring the complex structures that characterize enzymes in their components. The hierarchical self-assembly of peptides provides a means to create catalytic microenvironments. Ideally, as it occurs in enzymes, the catalytic activity of peptide nanostructures should be reversibly regulated. In a typical enzyme mimetic design, the peptide's self-assembling and catalytic activities are segregated into different regions of the sequence. Here, we aimed to design minimal peptides in which the self-assembly and function were all encoded in the same amino acids. Moreover, we wanted to endorse the resulting one-component nanomaterial with divergent, chemically unrelated, catalytic activities, a property not observed in natural enzymes. We show that short peptides consisting only of histidine and tyrosine residues, arranged in a binary pattern, form biocompatible amyloid-like fibrils and hydrogels combining hydrolytic and electrocatalytic activities. The nanofibers' mesoscopic properties are controlled by pH, the transition between assembled active β-sheet fibrils, and disassembled inactive random coil species occurring in a physiologically relevant pH range. The structure of one of such amyloid-like fibrils, as derived from molecular dynamic simulations, provides insights on how they attain this unique combination of structural and catalytic properties.

INTRODUCTION

Natural organisms use proteins and peptides self-assembly to build up a variety of mesoscopic materials, including collagen[1] and fibrin[2] in humans, spider silk,[3] or squid sucker ring teeth.[4] There is a rising interest in exploiting peptide self-assembly as a route to build up novel nanomaterials[5,6] since they might allow incorporating protein-like activity and responsivity to the environment into the nanostructure, providing control over the macroscopic and functional properties of the assembly. Besides, peptides can assemble under mild, close to physiological conditions, displaying excellent biocompatibility.

Amyloid fibrils belong to the group of ordered nanostructures that result from the self-assembly of polypeptides.[7] They have been traditionally associated with human diseases, but the recent discovery of amyloids assisting biological functions in a wide range of organisms, from bacteria to humans,[8,9] has changed this perception. Amyloid fibrils share a common quaternary structure, formed by the assembly of monomers into a characteristic "cross-β" structure, in which β-sheets are parallel to the fibril axis with their strands perpendicular to this axis.[10,11] This architecture is stabilized by hydrogen bonds between neighboring β-strands, and an array of other non-covalent contacts, like π-π stacking, van der Waals, electrostatic and hydrophobic interactions. This renders robust supramolecular structures without a need for exogenous cross-linking agents, a property exploited to design novel materials for biomedical and biotechnological applications.[5,12]

The buildup of materials via molecular self-assembly allows to define their ultimate structural and functional properties by designing the individual constituent molecules. A long-lasting objective in catalyst design has been to develop simple synthetic systems that can execute bio-inspired chemistry, without requiring defined and complex tertiary structures in the individual

molecules. The self-assembly of peptides provides a means for bringing multiple functional groups into proximity, in a way that is analogous to the folded conformation of enzymes.[13]

Catalytic self-assembled systems are typically modular, incorporating one or more amino acids relevant for the catalysis and a block responsible for the assembly, usually separated by a spacer.[14–16] The self-assembly promoting unit may or may not have a pure peptidic nature, like peptide amphiphiles, which are constructed by capping peptides with alkyl chains or other aromatic molecules. Both peptides and peptide amphiphiles have been successfully assembled into β-sheet-rich nanofibers able to hydrolyze activated esters, a typical model reaction for hydrolytic enzymes.[14,15] Like in many hydrolases, the active residue in the individual subunit is His[13,17,18] in some cases accompanied by an Arg to facilitate the catalysis.[14] Importantly, the architecture of the assembly provides an adequate enzyme-like microenvironment for the reaction, with the building blocks alone displaying low hydrolytic activity.[19] The same bottom-up strategy has been employed to obtain redox-active nanofibers, exploiting the reduction potentials that Tyr radicals acquire in assembled structures.[20,21] In several of these systems, when the concentration is increased, the peptide fibrils entangle to form a fibrillar network, which renders a hydrogel that retains the catalytic activity of the individual nanofibers.[19,22] The versatile properties of these hydrogels, such as high-water content and solid shape, have attracted great attention.[23]

The inherent sensitivity of polypeptide chains to pH is exploited by nature to control the structure of functional amyloids such as PMEL, a protein involved in melanin production, or the storage and secretion of pituitary peptide hormones. In both cases, the self-assembly into amyloid fibrils only occurs under the acidic conditions found in the respective granules.[24,25] Mimicking this strategy, pH-responsive peptide and peptide amphiphiles have been designed to develop new β-

sheet-based nanomaterials with tunable properties via a simple self-assembly mechanism without a need for exogenous cross-linking agents.[26,27]

pH-regulated peptide assembly offers an opportunity to mimic the behavior of natural enzymes in artificial nanofibrillar catalyzers, which might permit to regulate reactions simply by modulating the solution pH. Attaining this control is not trivial since it requires the integration of pH-responsiveness without interfering with the activity of catalytic residues. This has been achieved in a recent study by introducing a His residue at the terminus of a pH-responsive peptide.[19] The peptide exhibits a pH-dependent conformational transition from random coil to β-sheet and assembles into fibrils that display esterase activity. In this system, the activity could be reversed by pH-induced assembly/disassembly of the fibrils into random coils. This model system, and indeed most studies,[6,23,28,29] exploit the fact that amino acid side chains incorporating -COOH (Asp and Glu) or -NH_2 (Lys and Arg) groups can be in either a protonated or deprotonated state at pH values which are, respectively, below or above their nominal pKa values. Despite the pKa values in these self-assembling systems can be significantly shifted compared to solution ones,[30] the transitions necessarily occur far from the physiological pH.

It has just been reported that the assembly of the Orb2 protein into functional amyloids in *Drosophila melanogaster*[31] is governed by the protonation state of the imidazole group of His, a property shared by suckerin proteins in squids.[32,33] This suggests that, under physiological conditions, His residues might be used as molecular switches, endorsing synthetic peptides with self-assembly reversibility, in addition to catalytic activity, if they are embedded in the proper microenvironment.

We have recently designed a collection of synthetic prion-inspired heptapeptides.[21] These short peptides combine residues enriched in prion-like proteins (Asn, Gln, and Ser) with Tyr, the only

enriched aromatic residue in these polypeptides, forming a binary arrangement (Ac-XYXYXYX-NH_2). Despite their eminent polar nature, these peptides readily assembled into highly ordered amyloid fibrils.[21] Here we exchanged the polar residues in their sequences by His, obtaining a set of short peptides composed only by His and Tyr (hereinafter named as HY-peptides) consisting of 7, 8 and 9 residues, HY7 (Ac-HYHYHYH-NH_2), HY8 (Ac-YHYHYHYH-NH_2) and HY9 (Ac-HYHYHYHYH-NH_2), respectively. We rationalized that instead of having separate modules for assembly and function, the same residues might account for both activities in these peptides. We show that, indeed, HY-peptides present unique properties, since they assemble into biocompatible amyloid-like fibrils in a pH-dependent manner. These nanofibers act as multi-catalytic artificial enzymes because they combine both hydrolase and redox activities, thanks to their His and Tyr residues, respectively. The fibrils render active hydrogels at moderate peptide concentrations, whose assembled state can be controlled by the pH. Atomistic molecular dynamics simulations provide a structural explanation for this singular combination of conformational and functional features. Our results illustrate how supramolecular assemblies enable the incorporation of properties not seen in natural enzymes, such as the introduction of two different and unrelated catalytic activities into a single pH-regulated nanomolecular structure.

RESULTS AND DISCUSSION

HY-peptides self-assemble into amyloid-like structures at pH 8.0

The influence of pH on HY7, HY8 and HY9 peptides self-assembly was assessed by incubating each peptide at pH 4.0 or pH 8.0. The assembly was first monitored through synchronous light scattering (**Figure S1A**). HY-peptides incubated at pH 8.0 exhibited a significant increase in the light scattering signal compared to those incubated at pH 4.0.

We investigated the secondary structure content of HY-peptides incubated at pH 8.0 and pH 4.0 by circular dichroism (CD) spectroscopy (**Figure S1B**). The far-UV CD spectra of peptides incubated at pH 8.0 presented a minimum at 217 nm associated with β-sheet structures. In contrast, in HY-peptides incubated at pH 4.0, the signal gradually decreased at low wavelengths, a feature assigned to random coil conformations, suggesting that HY-peptides remained disordered at this pH. At both pHs, the peptide spectra exhibited positive maxima around 230 nm, arising from the contribution of the peptide aromatic side chains.[34] These signals decreased and were redshifted at pH 8.0 relative to those at pH 4.0.

Next, we assessed the secondary structure of the assemblies formed upon incubation at pH 8.0, by Fourier-Transform Infrared (FTIR) spectroscopy and recording absorbance in the amide I region of the spectrum (**Figure S1C and Table S1**). In addition to a peak at ~1610 cm^{-1} corresponding to His and Tyr aromatic side chains, the FTIR spectra were dominated by a signal comprised between 1615 and 1632 cm^{-1}, accounting for ~ 70 % of the total area of the absorbance spectrum for all HY-peptides. This signal can be assigned to intermolecular β-sheet structure. We could not detect antiparallel β-sheet signals at ~1690 cm^{-1}, suggesting a preferential parallel

disposition of the β-strands in the assemblies. The FTIR and CD data are in good agreement, indicating the formation of β-sheets when HY-peptides are incubated at pH 8.0.

We assessed if these β-sheet enriched assemblies exhibited an amyloid-like signature using the amyloid-specific dyes Thioflavin-T (Th-T) and Congo Red (CR). Th-T was added to HY-peptides incubated at pH 4.0 or pH 8.0 for 4 days. As shown in **Figure 1A**, the three peptides promoted an increase in the Th-T fluorescence signal only at pH 8.0, whereas the spectra of samples incubated at pH 4.0 resembled that of the buffer with Th-T only. Binding to CR confirmed the differential behavior of the peptides at the two pHs. As shown in **Figure 1B**, HY-peptides incubated at pH 8.0 showed a red-shift of the respective CR absorption spectra, while the peptides incubated at pH 4.0 presented a spectrum similar to that of the buffer with CR. Thus, both assays indicate that the peptides form amyloid-like assemblies only when incubated at alkaline pH.

The morphology of the assemblies was visualized by transmission electron microscopy (TEM). Analysis of representative micrographs revealed the presence of small amorphous assemblies in HY-peptides incubated at pH 4.0. In contrast, samples incubated at pH 8.0 displayed long and thin fibrillar structures (**Figure 1C**), consistent with an amyloid-like nature, although they differed in morphology between peptides. We measured the thickness of the imaged HY7, HY8 and HY9 fibrils at pH 8.0 using high magnification micrographs (**Figure 1C**) displaying widths corresponding to 16.5 ± 4.0 nm, 21.0 ± 6.4 nm and 7.2 ± 1.2 nm, respectively, in agreement with the dimensions reported for different amyloid structures.[35]

The analysis of the peptides incubated at pH 8.0 by dynamic light scattering (DLS) confirmed the presence of large assemblies (**Figure S2**). On the contrary, samples incubated at pH 4.0 did not show any evident DLS signal since species' sizes were under the detection range of the instrument. The average diameter of HY-peptides assemblies at pH 8.0 was 1031.0 ± 453.8 nm

(HY7), 3161.4 ± 1004.2 nm (HY8), and 2097.9 ± 940.2 nm (HY9). Although these dimensions are in the range observed by DLS for different amyloid assemblies,[36,37] they should not be taken as a proxy of the fibril length since DLS is only accurate in measuring dimensions of spherical particles, and they just reflect the relative sizes of the different assemblies. The sizes were not monotonically increasing with the length of the peptide chain. We hypothesized that this might respond to the fact that HY7 and HY9 have a composition of $H_{n+1}Y_n$, whereas HY8 composition formula is H_nY_n. To explore this possibility, we synthesized an HY6 peptide (Ac-HYHYHY-NH_2).

At pH 8.0, HY6 forms assemblies that bind to Th-T **(Figure S3A)** and CR **(Figure S3B)**, exhibit high β-sheet content as measured by FTIR **(Figure S3C** and **Table S1)** and appear as highly ordered fibrils, 19.0 ± 4.9 nm in width **(Figure S3D)**. As expected, HY6 does not assemble into amyloid-like structures at pH 4.0 (**Figure S3**). DLS analysis, indicated that, as hypothesized, the diameter of HY6 assemblies at pH 8.0 (765.6 ± 120.5 nm) was smaller than the one of HY8 ones (**Figure S2**).

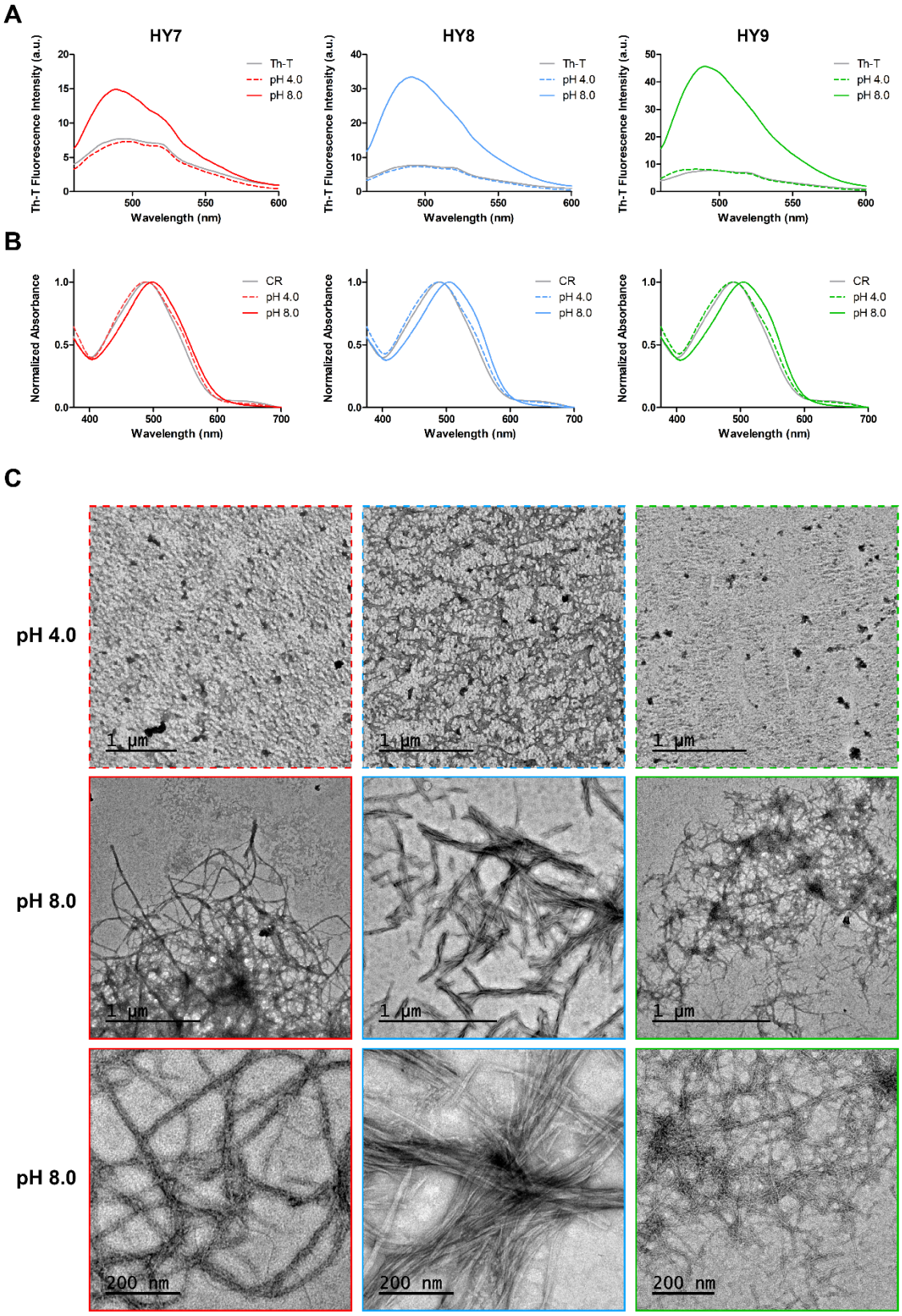
A
HY7
HY8
HY9
Th-T Fluorescence Intensity (a.u.)
Wavelength (nm)
Th-T
pH 4.0
pH 8.0
B
Normalized Absorbance
CR
pH 4.0
pH 8.0
C
pH 4.0
pH 8.0
pH 8.0
1 μm
200 nm

Figure 1. Characterization of the amyloid-like properties for HY-peptides incubated at pH 4.0 and pH 8.0. The amyloid tinctorial properties of HY7 (red), HY8 (blue) and HY9 (green) incubated peptides were assayed using **A)** Th-T and **B)** CR. Spectra in the absence (grey line) and in the presence of HY7 peptides incubated at pH 4.0 (dashed line) and at pH 8.0 (solid line) are shown. **C)** Representative micrographs of HY-peptides samples incubated at pH 4.0 (dashed line, upper row) and at pH 8.0 (solid line, middle and bottom rows). Scale bars correspond to 0.2 or 1 μm.

HY-peptides fibrils are innocuous for human cells

One of the limitations of amyloid-like materials is that they might possess certain cytotoxic activity.[38] In order to discard this possibility, HY amyloid-like fibrils formed at pH 8.0 were isolated by centrifugation and added to SH-SY5Y neuroblastoma cultured cells at concentrations ranging between 10 and 50 μM (**Figure S4**). After 72 hours, the cell viability was monitored using the PrestoBlue® reagent. None of the fibrillar assemblies display significant cytotoxicity at any of the tested concentrations, suggesting that they would have a good biocompatibility.

Amyloid self-assembly of HY-peptides is controlled by pH

The results presented above converge to indicate that the fibrillation of HY-peptides under mild conditions is strongly dependent on pH. We assessed if the degree of peptide self-assembly correlates with the solution's pH. HY-peptides were incubated at pHs ranging from 4.0 to 8.5 in Tris-Citrate buffer (**Figure 2**). Amyloid formation was monitored using Th-T. Since the peptide termini are protected by amidation and acetylation modifications and the tested pH range should not affect Tyr's protonation (L-Tyr side chain pK_a = 10.5); the behavior of these peptides would be directly associated to the protonation state of their His residues (L-His side chain pK_a = 6.0).

As shown in **Figure 2**, the three HY-peptides exhibited a pH-dependent transition with a $pH_{1/2}$ which is close to the pKa value of 6.88 determined for the imidazole group of histidine in the random-coil peptide Ac-Ala-Ala-His-Ala-NH_2[39] (**Table S2**), indicating that His deprotonation facilitates self-assembly, whereas electrostatic repulsion between positively charged His impedes it. There exist subtle differences in the $pH_{1/2}$ between the peptides, with HY7 and HY9 pH transitioning at slightly higher pH than HY8. This might owe to the different His/Tyr ratio in the peptides, the identity of the C-terminal residue, or to a different environment of the His residues in the different assemblies.

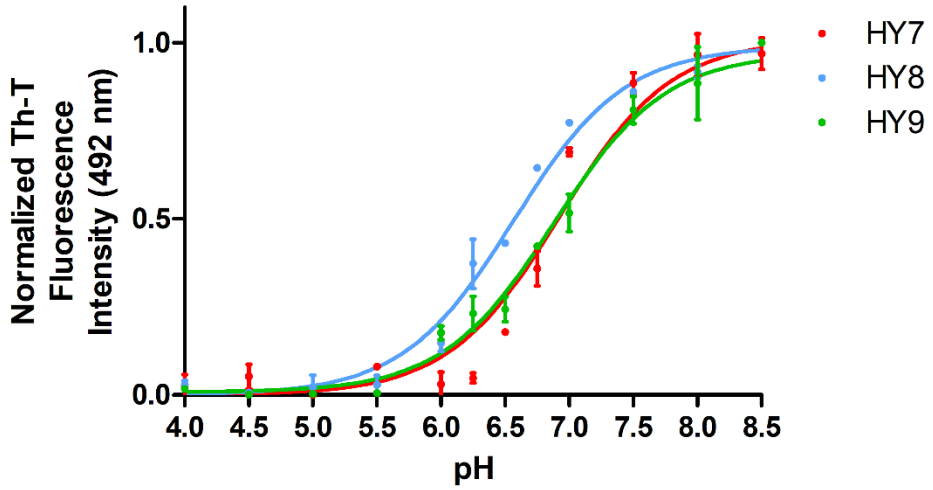

Figure 2. HY7, HY8, and HY9 peptides self-assembly as a function of the pH. HY7 peptide (red line) was measured at 200 μM final concentration and HY8 (blue line) and HY9 (green line) peptides were assayed at 100 μM final concentration in 100 mM Tris HCl 50 mM Citrate buffer adjusted at different pHs (4.0 to 8.5 each 0.5 pH units) and the assembled state evidenced by the addition of Th-T. Th-T maximum emission at 492 nm was recorded, and fluorescence intensity normalized. Fitting of the data to a sigmoidal curve was performed using GraphPad Prism 5.0

software. Data correspond to the mean of three independent experiments and error bars indicate standard deviation.

pH-responsive HY-peptides amyloids

The properties of HY-peptides suggested that they might experiment bidirectional assembly/disassembly in response to changes in the pH, which would allow to control their supramolecular state. To assess if this was the case, HY-peptides were initially self-assembled at pH 8.0 for 4 days and then the solution was acidified to pH 4.0 and allowed to stand for 4 days. Finally, the pH was reverted again to pH 8.0 and the peptides solution incubated for 4 additional days.

The process was monitored simultaneously by synchronous light scattering, far-UV CD, Th-T and CR binding (**Figure 3**). The results from synchronous light scattering, Th-T, and CR binding converged to indicate that the amyloid-like assemblies formed at pH 8.0 were disassembled at pH 4.0 and that upon reversion to pH 8.0 the amyloid properties were at least partially recovered (**Figure 3A, 3B and 3C**). The CD spectra of the HY-peptides revealed that the minimum signal detected at 217 nm corresponding to β-sheet present in samples incubated at pH 8.0 disappeared at pH 4.0, and then was recovered back when the pH turned alkaline (**Figure 3D**).

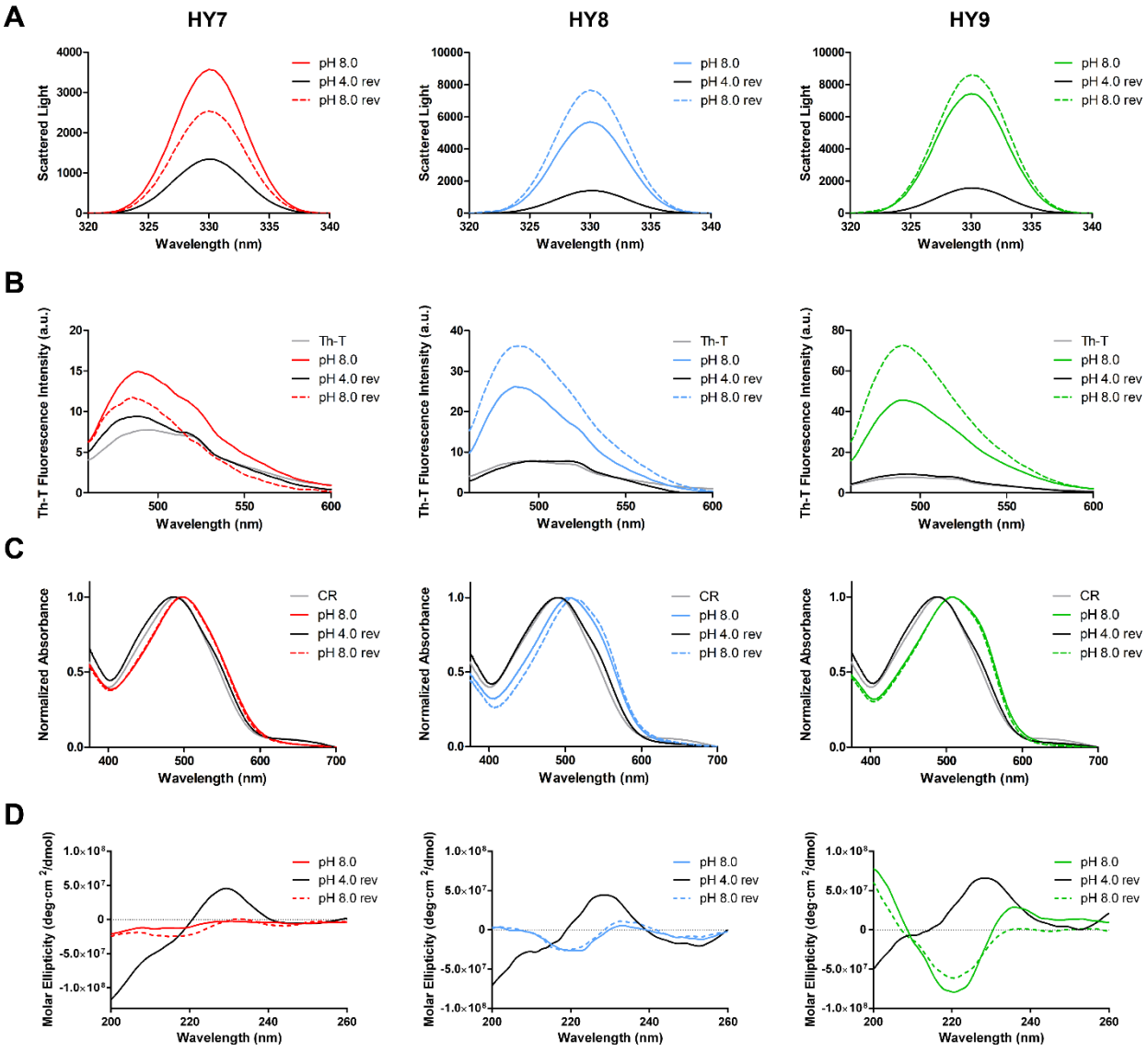

Figure 3. HY7, HY8, and HY9 peptides assembly, disassembly and reassembly as a function of the pH. HY7 (red), HY8 (blue), and HY9 (green) peptides were prepared at 250 μM. An initial self-assembling incubation step was performed at pH 8.0 (solid colored line), followed up by a disassembling incubation step at pH 4.0 (solid black line), and a re-assembling incubation step induced at pH 8.0 (dashed colored line). **A)** The aggregated state of the samples was analyzed by synchronous light scattering. Amyloid tinctorial properties were assessed by **B)** Th-T and **C)** CR

binding assays, performed in the absence (grey line) and in the presence (colored and black lines) of peptide. **D)** The secondary structure content of the peptides was assessed by far-UV CD.

The peptide solutions were imaged at each step by TEM. As shown in **Figure S5**, HY-peptides incubated at pH 8.0 displayed an amyloid-like fibrillar morphology, whereas upon acidification to pH 4.0, fibrils were no longer present and only small and dispersed amorphous aggregates were observed. In good agreement with the above biophysical data, reversion to pH 8.0 promoted the re-organization into fibrillar assemblies, despite their morphology was less regular than the original ones.

We used HY8 as a model system to test if the transition between a non-amyloid state at pH 4.0 and an amyloid-like ensemble at pH 8.0 is sustained after several cycles of acidification-alkalinization. **Figure S6** shows that this is the case for at least 4 cycles.

The data converge to indicate that the soluble/assembled transitions observed for HY peptides depend on the ionizable imidazole side chains, and indeed, a QY7 peptide (Ac-QYQYQYQ-NH_2) which, as HY-peptides, forms amyloid fibrils at pH 8.0[21] retains its aggregated state and amyloid-like properties when the solution is acidified to pH 4.0 (**Figure S7**).

HY8 peptide forms a pH-responsive hydrogel

We selected the HY8 peptide as a model and assessed if it can form a mechanically rigid and reversible hydrogel at higher concentrations (**Figure 4**). The inverted tube test indicates that when the peptide is incubated at 5 mM (0.5 % w/v) and pH 4.0, the solution remains liquid, but upon alkalization to pH 8.0 and incubation for 4 days a rigid hydrogel matrix is formed. Hydrogelation is reversible and lowering the pH to 4.0 causes the gel to fluidize immediately.

Other β-sheet-based nanomaterials able to switch between soluble and assembled states as a function of the pH have been described previously; however, because they either exploit Asp and Glu (pKa < 4.5) or Lys and Arg (pKa > 10) residues, the transitions between states occur further from the physiological pH than in our case.[6,23,28,29]

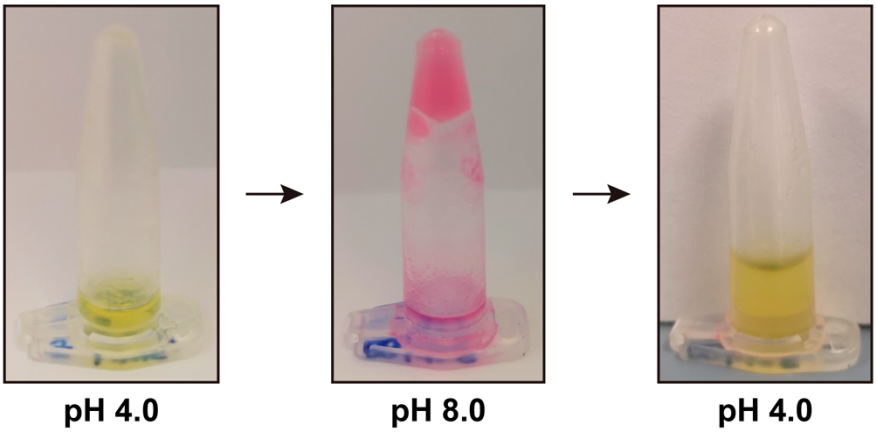

Figure 4. pH-reversible transition of HY8 from solution to hydrogel. The HY8 peptide was initially incubated at pH 4.0 in the presence of phenol red pH indicator, which presents a yellow colour at this pH (left image). Upon increase of the pH to 8.0, phenol red shifts to red/pink colour and a solid hydrogel is formed (middle image). Decreasing the pH to 4.0 disentangles the formed hydrogel and turns the pH indicator yellow again (right image).

HY-peptides amyloid-like fibrils display esterase activity

The imidazolyl groups of His are present at the active sites of many hydrolytic enzymes, like trypsin[40] and chymotrypsin.[41] Peptides containing His residues have been assembled into nanofibers that function as mimics of biological hydrolytic enzymes, catalyzing ester hydrolysis.[14,15] In HY-peptides fibrils, at least 50% of the residues are His, suggesting that they

might also exhibit esterase activity. To address this possibility, HY-peptides fibrils were incubated in the presence of the commonly employed substrate p-nitrophenyl acetate (pNPA), which hydrolysis produces p-nitrophenol (pNP), a chromogenic molecule, that can be monitored by measuring the increase in absorbance at 405 nm. As in biological enzymes, the imidazole is expected to react with the pNPA to form phenol and acylium ion imidazole complexes. The complex would then react with water to form acetic acid and regenerate the imidazole ring.

Kinetic assays at pH 8.0 revealed that HY-peptides were able to catalyze ester hydrolysis without any additional co-factor. We calculated the kinetic parameters of the reaction. The initial pNPA hydrolysis rates were measured as a function of the substrate concentration, maintaining the concentration of peptide fibrils constant (**Figure 5A**). Double-reciprocal plots were obtained **(Figure S8),** and the apparent kinetic constants calculated according to the Michaelis-Menten equation. The different peptide fibrils did not present large differences in their kinetic parameters (**Table S3**), with $k_{cat(app)}/K_M$ specificity constants of 1.26 ± 0.43 M^{-1} s^{-1}, 1.36 ± 0.18 M^{-1} s^{-1} and 1.64 ± 0.33 M^{-1} s^{-1}, for HY7, HY8 and HY9 peptides, respectively. The typical enzymatic saturation kinetics shown by these scaffolds indicates that they behave as actual enzymes. Kinetic parameters were also calculated at pH 7.4 **(Figures S9 and S10)**, as expected, the fibrils were slightly less active than at pH 8.0 (**Table S3**), with $k_{cat(app)}/K_M$ values of 0.47 ± 0.49 M^{-1} s^{-1}, 0.54 ± 0.19 M^{-1} s^{-1} and 0.55 ± 0.37 M^{-1} s^{-1} for HY7, HY8 and HY9 peptides, respectively.

No connection between the peptide length and the catalytic activity was evident, as previously described for the Zn^{2+} dependent esterase activity of related amyloid peptides.[18] Among the reported catalytic peptide assemblies for ester hydrolysis, metal-chelated higher-order constructs exhibit the highest activities.[13,17,42] HY-peptides' activity was in the same range as that of non-metal dependent catalytic nanofibrils at the same pH.[14]

We have shown that HY8 forms a hydrogel and that the phase behavior can be tightly controlled by the pH. We addressed if the fibrils entangled in the gel state display esterase activity (**Figure 5B**). A HY8 gel was prepared at pH 8.0 and 5 mM peptide concentration. A 20 µL aliquot of pNPA was then added into the hydrogel. After few minutes the gel acquired the yellow coloration of the pNP product, a clear indication that the nanostructure was catalytically active.

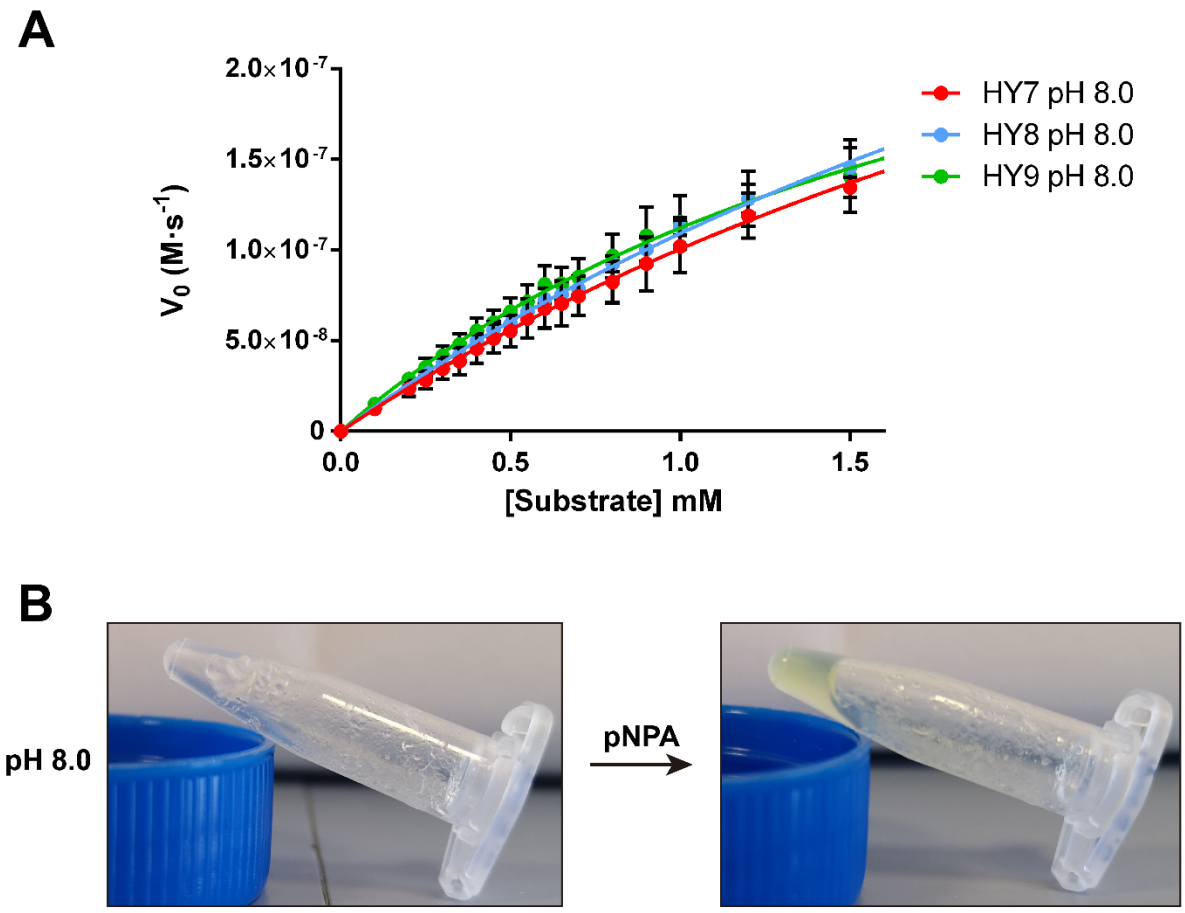

Figure 5. Esterase activity characterization. **A)** HY7, HY8 and HY9 esterase activity was detected by measuring the absorbance of the yellow-colored pNP product at 405 nm in 25 mM Tris-HCl pH 8.0 (E_0 concentration 100 µM). Data were fitted to the Michaelis-Menten equation with GraphPad PRISM 5.0 software. **B)** HY8 hydrogel esterase activity. HY8 peptide was

incubated at 5 mM at pH 8.0. An aliquot of 1 mM pNPA was added and the sample incubated for 30 minutes (right image). The yellow color indicates the production of chromogenic pNP.

HY-peptides amyloid-like fibrils are electrochemically active

In biological systems such as the photosystem II, Tyr acts as redox-active residue thanks to its location in chemical environments that reduce the activation potentials for the generation of tyrosyl radicals.[43] In solution, L-Tyr can generate tyrosyl radicals, but those are rapidly quenched in an aqueous solvent. Over the past few years, different studies have created redox-active scaffolds by incorporating Tyr residues into peptidic building blocks.[20,44] We rationalized that the defined chemical environment of HY-peptides fibrils might endorse their Tyr radicals with reduction potentials high enough to catalyze chemical reactions.

We explored if HY-peptides fibrils can act as bioelectrocatalysts by assessing the oxidative polymerization of pyrrole as a model reaction.[45] Polypyrrole (PPy) can be synthesized electrochemically by applying a potential greater than 0.8 V vs. Ag/AgCl or chemically by using an oxidant agent. Although electropolymerization can be initiated at 0.8 V vs. Ag/AgCl, the rate at this potential is too slow to attain macroscopic PPy deposition. Our results showed that at 0.8 V vs. Ag/AgCl, a negligible amount of PPy was produced in the presence of L-Tyr (10 μA at 500 seconds) (**Figure 6A and Figure S11**). In contrast, when this voltage was applied to HY7, HY8, and HY9 fibrils, the chronoamperometry curves indicated that pyrrole polymerized rapidly, in the range of seconds. Intensities of 850 μA were attained for HY8 and HY9 fibrils and 400 μA for HY7 ones. Continuous deposition of PPy was observed in all cases (**Figure 6A**). The lower bioelectrocatalytic activity of the HY7 peptide might respond to its inferior self-assembly propensity or to the fact that it contains only 3 Tyr residues instead of the 4 Tyr in HY8 and HY9.

We investigated whether HY-peptide fibrils would allow Cu(II) ions to oxidize pyrrole and thus promote PPy formation through tyrosyl mediated electron transfer, without applying any additional potential. The fibrils were dissolved in a 4 mM $CuCl_2$ solution and exposed to pyrrole vapor (**Figure 6B**). Solutions containing L-Tyr and $CuCl_2$ or $CuCl_2$ only were used as controls. In agreement with the electrochemical studies, after incubation for 16 hours, only the peptide containing tubes exhibited a black material, corresponding to PPy that precipitated together with the fibrils **(Figure 6C and Figure S11)**. Consistent with their bioelectrocatalytic activities, the quantification of the generated PPy for each peptide by absorbance showed a higher capacity to generate PPy for HY9 and HY8 respect to HY7 chemically (**Figure 6C**).

When the above described experiments were performed with HY7, HY8 and HY9 peptides incubated at pH 4.0, no electrochemical or Cu(II)-mediated pyrrole oxidizing activity was evident (**Figure S12**).

The results in this section indicate that, as in the case of His, the chemical environment of Tyr in the HY-peptides amyloid fibrils allows them to contribute to biocatalysis.

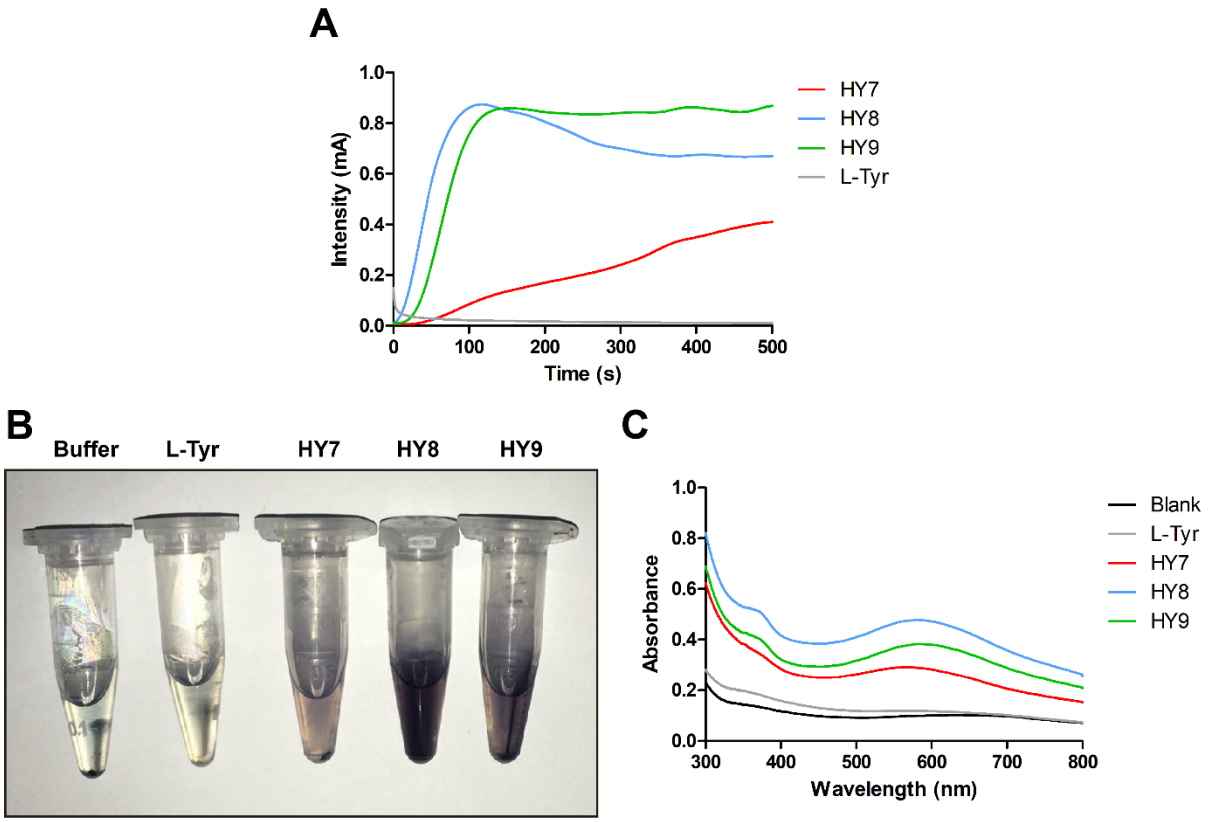

Figure 6. HY7, HY8, and HY9 fibrils act as bioelectrocatalyst. **A)** Chronoamperometry (CA) curves of the electropolymerization of polypyrrole (PPy) using HY7 (red line), HY8 (blue line), HY9 (green line) fibers and monomeric L-Tyr (grey line). Potential applied at 0.8 V vs Ag/AgCl in 0.1 M NaCl containing 50 mM pyrrole and 250 μM peptide fibrils or 250 μM L-Tyr. **B)** Image of the centrifuged tubes corresponding to the chemical polymerization after 16 hours exposition to distilled pyrrole vapor. **C)** Graphs corresponding to the UV-Vis absorbance spectra of the generated PPy. Spectra were acquired from 300 to 800 nm. Control tubes contain $CuCl_2$ (black line) and L-Tyr (grey line).

Atomistic simulations of HY8 peptide amyloid-like structures.

To gain structural insight on HY-peptides' pH-responsiveness, we selected HY8 as a model and performed atomistic molecular dynamics simulations (see Supplementary Information for computational details). As FTIR results suggest that self-assembly leads to the formation of parallel β-sheets, we explored the six possible parallel steric zippers arising from HY8 aggregation,[11] probing the whole range of side chain distributions at the interface between two parallel β-sheets (**Figure S13**). These models can be classified into three main families: i) those that pack only histidine residues at the steric zipper, leaving tyrosines exposed to the solvent, ii) those that pack only tyrosines at the interface, leaving out histidines, and iii) mixed systems where both tyrosines and histidines coexist at the steric zipper. Since our simulations target fibrillar structures at an atomistic level, we had to account for the two possible tautomers - δ-nitrogen protonated and ε-nitrogen protonated - of histidine at neutral pH. Each parallel steric zipper architecture was built with all histidines in either one of the two tautomeric states, leading to fully δ-nitrogen protonated (HY8d) and fully ε-nitrogen protonated (HY8e) models. We then compared the relative stability of all models for each tautomeric state (see Supplementary Information). Results show that the preferred arrangement for both HY8e and HY8d fibrils involves packing of histidines at the steric zipper (P-FF1-UD), leaving tyrosines exposed to the solvent (**Figure 7A**). Analysis of intersheet non-covalent interaction integrals[46] indicates that this preferred architecture for HY8e is the one that maximizes side chain packing at the interface (**Table S4 and S5**).

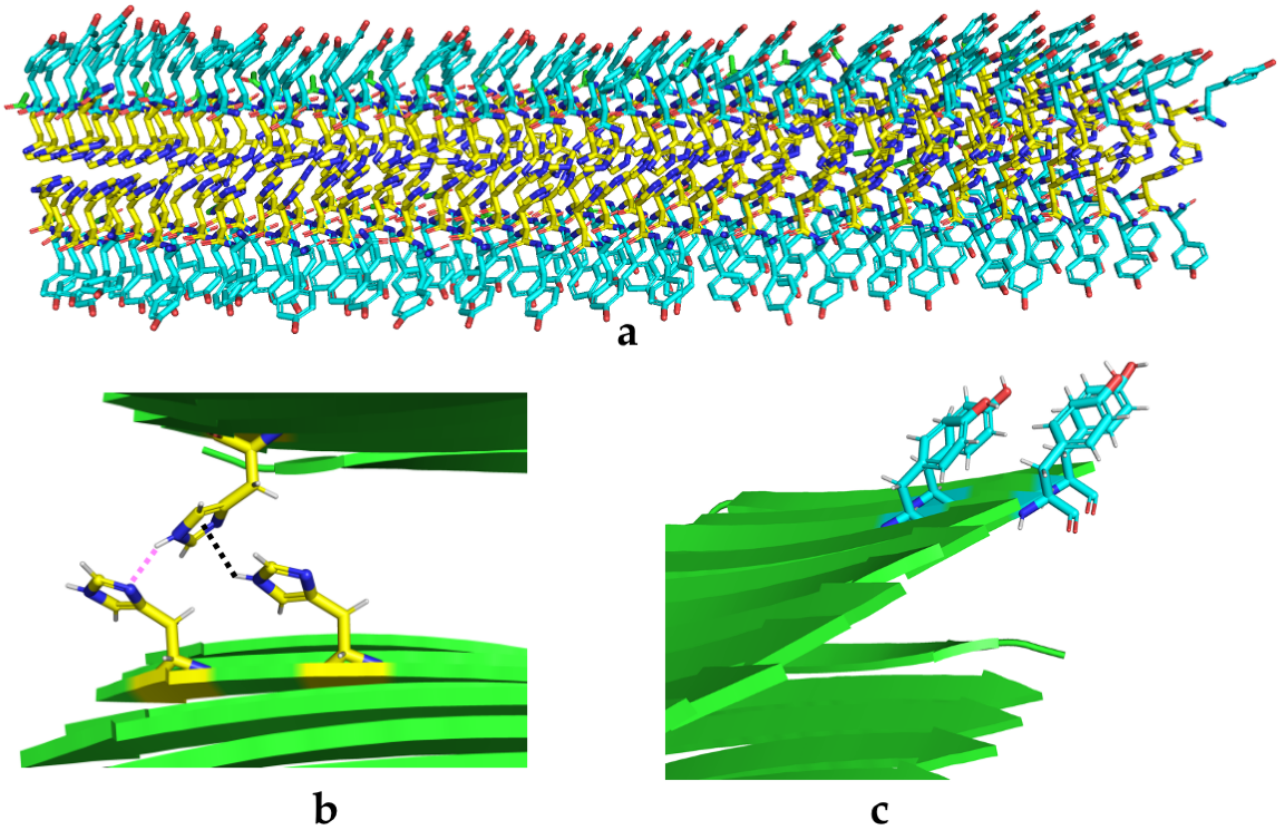

Figure 7. A) Structural model of the preferred ε-protonated steric zipper organization of HY8 amyloid-like fibrils (HY8e-P-FF1-UD), **B**) steric zipper histidine-histidine interactions, and **C**) tyrosine side chains exposed to the solvent.

Main inter-β-sheet contacts between histidine side chains include dispersion and N-H/C-H···π interactions (**Figure 7B**). This is likely to produce a network of cooperative hydrogen bonds that contribute to fibril stability. The pH-dependent behavior of HY8 self-assembly can be explained in terms of the availability of singly protonated histidine residues for establishing stabilizing contacts at the steric zipper. Lowering the pH, an increasing fraction of histidine residues will be doubly protonated, bearing a positive charge, and hindering fibril formation due to electrostatic

repulsion. Increasing the pH, histidines lose the positive charge and can be engaged in the zipper fibril formation, which would explain the pH-responsiveness HY-peptide amyloid.

While our simulations predict the preferred arrangement of the bilayer – the basic unit of the aggregate – they cannot predict the global morphology of the fibril; indeed, both imperfections in the growth mechanism and the supramolecular assembly of individual steric zippers can fine-tune fibrillar architectures through subtle energy changes. Thus, while we predict that Tyr are the more likely residues to be exposed to the solvent, and consequently the more available for catalysis, we cannot exclude that also His residues can be exposed, either through lateral offsets between steric zipper layers or hybrid bilayer organization. Indeed, it has already been shown that fibril polymorphism can occur even at the level of short peptides with repeating units.[47]

CONCLUSIONS

In this study, we designed de novo short peptides containing only His and Tyr residues in a binary pattern to form biocompatible amyloid-like nanofibers that act as enzyme mimetics and exhibit two different and unrelated catalytic activities. His residues provide the contacts that sustain the parallel β-sheet amyloid zipper and endorse the fibrils with hydrolytic activity, whereas Tyr residues stabilize the exterior of the bilayer by a ladder of aromatic ring packing, allowing to perform electrocatalytic reactions. This structure/function duality is in stark contrast with most peptide-based catalytic materials designed to date, which exploit a modular architecture with different blocks accounting for the assembly and the activity, making them necessarily more complex. The fact that the imidazolyl groups of His contribute the interactions sustaining the inner steric zipper makes them pH-responsive, their reversible conformational transition being regulated by pH changes. In contrast to most pH-responsive β-sheet fibrils reported to date, the mechanical properties transition occurs in a physiological pH range, as it happens in pH-responsive natural amyloids.[31–33] Analogously to enzymes catalytic sites, it is the three-dimensional fibril microenvironment that permits the catalytic activity. This allows forming catalytically active stiff hydrogels at moderate peptide concentrations, where the product can be potentially separated by inducing a gel-to-solution transition. Thus, in HY-peptides, form follows function.

Overall, we show how a short peptide with a very low sequence complexity can assemble in a pH-dependent manner and in the absence of cofactors into an enzyme mimetic nanomaterial displaying two divergent catalytic activities. To the best of our knowledge, this combination of structural and catalytic properties has not been previously described in designed or natural enzymes. This bottom-up strategy lays the foundations to generate "smart" nanostructured materials, with a la carte combinations of catalytic functions for practical applications. In order to

scale up the production of this kind of novel bio-catalyzers, their preparation from small unmodified peptides is advantageous because they can be straightforwardly prepared via solid-phase synthesis with precise control over the sequence and molecular dimensions, low cost, and high biocompatibility.

MATERIALS AND METHODS

Peptides preparation. Synthetic peptides, HY6 (Ac-YHYHYH-NH_2), HY7 (Ac-HYHYHYH-NH_2), HY8 (Ac-YHYHYHYH-NH_2) and HY9 (Ac-HYHYHYHYH-NH_2) were purchased from RoyoBiotech Co. ltd. (Shanghai, China). The peptides were N-terminal acetylated and C-terminal amidated, to avoid the effect of the terminal charges, mimicking a protein sequential context. Lyophilized peptides were dissolved in 1,1,1,3,3,3-hexafluoro-2-propanol (HFIP) to obtain a 10 mM stock solution, aliquoted and frozen at -80°C. For hydrogel formation, HY8 peptide stock solution was prepared as described above at a final concentration of 20 mM, aliquoted and frozen at -80°C.

Dependence of the peptides self-assembly on the pH. HY7 peptide was diluted from 10 mM stock to 200 μM and HY8 and HY9 peptides were diluted from 10 mM stock to 100 μM in 100 mM Tris, 50 mM Citrate buffer at different pH (4.0, 4.5, 5.0, 5.5, 6.0, 6.5, 7.0, 7.5, 8.0 and 8.5). Independent triplicates were prepared. For each peptide, the ten solutions were incubated at room temperature and quiescent conditions for 24 hours and then analyzed by fluorescence spectrophotometry diluting to 25 μM final concentration and adding Th-T amyloid binding dye at 25 μM in MilliQ H_2O. Th-T emission fluorescence was detected on a Jasco FP-8200 fluorescence spectrophotometer (Jasco Corporation, Japan) in the range 460-600 nm, using an excitation wavelength of 445 nm, with excitation and emission bandwidths of 5 nm. The signal at 492 nm was recorded to obtain the pH dependence curves. Data were normalized and curves were fitted using a non-linear fitting to the Henderson-Hasselbalch equation in GraphPad Prism 5.0, obtaining the $pH_{1/2}$ values for each peptide. Data correspond to the mean of three independent experiments and error bars correspond to standard deviation.

Peptides aggregation. HY6, HY7, HY8, and HY9 peptides were diluted from 10 mM stock to 250 μM final concentration in 100 mM Tris HCl pH 8.0 buffer and in 100 mM Tris HCl, 50 mM Citrate pH 4.0 buffer, and reactions were incubated 4 days at room temperature in quiescent conditions.

Peptide assembly, disassembly and reassembly reactions. HY7, HY8, and HY9 peptides were diluted from 10 mM stock to a final concentration of 250 μM in 100 mM Tris, 50 mM Citrate pH 8.0 and incubated for 4 days at room temperature in quiescent conditions for peptide aggregation. After the initial aggregation reaction incubation, pH was modified to 4.0 with the addition of a small amount (approximately 5 μL) of concentrated 37% HCl solution (Sigma Aldrich, Germany) and samples were incubated for 4 days at room temperature and quiescent conditions for disaggregation. To promote reaggregation, a small amount of 5 M NaOH solution was added to the reactions to increase the pH to 8.0 (approximately 5 µL). Samples were then incubated for 4 days at room temperature and quiescent conditions for the reassembling of the fibrils.

HY8 peptide was exposed to a total of 4 assembling-disassembling cycles by pH modulation between pH 8.0 and pH 4.0. Acidification was promoted by the addition of 5 to 10 µL of hydrochloric acid and pH was checked with a pH-meter. Alkalinization was promoted by the addition of 5 to 10 µL of 10 M NaOH solution and pH was checked with a pH-meter. Samples were incubated in each cycle for 4 days to promote the assembly/disassembly of the fibrils and analyzed as previously described.

QY7 assembly and disassembly reaction. QY7 peptide was previously demonstrated to form highly stable fibrils under physiological conditions.[21] QY7 peptide was incubated in 100 mM PO_4 buffer at pH 8.0 for 7 days. Then, the sample was split in two tubes and centrifuged at 12,000 x g for 30 minutes. Pelleted fibrils were resuspended in the same volume of 100 mM PO_4 buffer at pH

8.0 or in 100 mM Tris HCl 50 mM Citrate buffer at pH 4.0. The reactions were incubated for 2 days. The samples were analyzed by measuring the Th-T, CR and light scattering spectra as described above.

Amyloid dyes binding. Thioflavin T (Th-T) and Congo Red (CR) dyes were used to determine amyloid fibers formation. For Th-T binding assay, incubated peptides were diluted to a final concentration of 25 μM in MilliQ H_2O and Th-T was added to a final concentration of 25 μM. Th-T emission fluorescence was detected on a Jasco FP-8200 fluorescence spectrophotometer (Jasco Corporation, Japan) in the range 460-600 nm, using an excitation wavelength of 445 nm and with excitation and emission bandwidths of 5 nm. For CR binding assay, incubated peptides were diluted 1:10 in MilliQ H_2O and CR was added to a final concentration of 10 μM. Optical absorption spectra were recorded from 375 to 700 nm in a Specord200 Plus spectrophotometer (Analytik Jena, Germany). Spectra of protein alone were acquired to subtract protein scattering.

Light scattering. HY-peptides were diluted to a final concentration of 25 μM and light scattering was measured in a Jasco FP-8200 fluorescence spectrophotometer (Jasco Corporation, Japan), exciting at 330 nm, and recording in the range 320-340 nm using an excitation and emission bandwidth of 5 nm.

Circular dichroism (CD). CD spectra were acquired in a Jasco J-715 Spectropolarimeter (Jasco, Japan). HY7, HY8, and HY9 peptides were diluted from the incubated reaction to 50 μM in MilliQ H_2O. CD spectra measurements were performed in the far-UV range (260-200 nm) in a 1 mm path-length polarized quartz cuvette, with standard sensitivity, 1 nm bandwidth, 1 second response, 0.5 nm data pitch and 100 nm/min speed. Spectra were recorded at 25°C. The final spectrum is the result of 10 spectrums average and subtraction of buffer spectrum.

Fourier Transform Infrared (FTIR) spectroscopy. Secondary structure conformation was assessed by means of Attenuated Total Reflectance-Fourier Transform Infrared (ATR-FTIR) spectroscopy. Assembled HY7, HY8, and HY9 fibers were centrifuged at maximum speed 12,000 x g for 30 minutes and resuspended in MilliQ H_2O. Samples were placed on the ATR diamond crystal and dried out with nitrogen flow. The experiments were carried out in a Bruker Tensor 27 FTIR (Bruker Optics, United States) supplied with a Specac® Golden Gate MKII ATR accessory. Each spectrum consists of 32 acquisitions measured at a resolution of 1 cm^{-1}. Data were acquired and normalized using the OPUS MIR Tensor 27 software (Bruker Optics, United States). FTIR spectra were fitted employing a nonlinear peak-fitting equation using PeakFit package v4.12 (Systat Software, United States). The area for each Gaussian curve was calculated in the amide I region from 1700 to 1600 cm^{-1} using the second derivative deconvolution method in PeakFit package v4.12 (Systat Software, United States).

Transmission Electron Microscopy (TEM). HY6, HY7, HY8, and HY9 incubated samples were deposited over carbon-coated copper grids for 10 minutes. Sample excess was dried with a filter paper and negative staining was applied over the samples incubating 5 μL of 2 % (w/v) uranyl acetate for 1 minute and excess was dried out again with filter paper. Grids were exhaustively scanned using a JEM 1400 transmission electron microscope (JEOL Ltd, Japan) operating at 80 kV and images were acquired with a CCD GATAN ES1000W Erlangshen camera (Gatan Inc, United States).

Determination of HY6, HY7, HY8 and HY9 fibrils width. TEM micrographs were analyzed to determine width of HY6, HY7, HY8, and HY9 fibrils. Measurements were performed with ImageJ software (NIH, USA), using the corresponding scale. Values correspond to the mean of at least 20 different measurements from 3 micrographs. Error corresponds to the standard deviation.

Dynamic Light Scattering (DLS). Peptides reactions were prepared as described above and diluted 1:2 in the same buffer for its measurement. DLS measurements were performed at 25°C in a Malvern Zetasizer Nano S90 (Malvern, Worcestershire, UK). Each sample was measured 10 times, each time measured in 10 runs; average distributions are presented, and the standard deviation was calculated.

Cell viability assay. Human SH-SY5Y cells were plated into 96-well plates at a density of 4,000 cells/well (100 µL/well) in F-12 medium supplemented with 10 % FBS and maintained at 37°C and 5 % CO_2 atmosphere. HY7, HY8, and HY9 peptides were prepared at 250 μM in 100 mM Tris HCl pH 8.0 and in 100 mM Tris-Citrate pH 4.0 sterile buffers and incubated during 4 days at room temperature in quiescent conditions. After incubation, pH 8.0 samples were centrifuged at 12,000 x g for 30 minutes and soluble and insoluble fraction were separated. Pelleted fibrils were resuspended in the same volume of the previous buffer. Cells were incubated in the presence of 10, 25 and 50 µM of soluble and insoluble fraction for pH 8.0 samples and total fraction for pH 4.0 samples for 72 hours in triplicates. For controls, the same volume of 100 mM Tris HCl pH 8.0 buffer and 100 mM Tris-Citrate pH 4.0 buffer was added respectively in control wells.

Treated cells were incubated with 10 µL PrestoBlue® Cell Viability Reagent (Invitrogen, United States) for 30 minutes. Cell viability was determined by recording fluorescence at 615 nm, using an excitation wavelength of 531 nm in a Victor3 fluorescent plate reader (Perkin Elmer, United States). Data correspond to the mean of two independent experiments and error bars correspond to standard deviation.

Esterase activity assay. HY7, HY8, and HY9 peptides were prepared at 250 μM in 100 mM Tris HCl pH 8.0 buffer and incubated for 4 days at room temperature in quiescent conditions. Samples were centrifuged at 12,000 x g for 30 minutes and the supernatant was removed. For

assays at pH 8.0, pelleted fibers were resuspended in 25 mM Tris HCl pH 8.0. Esterase activity assay was performed 100 μM peptide final concentration for all the assays. For assays at pH 7.4, pelleted fibrils were resuspended in 25 mM Tris HCl at pH 7.4. The reaction was performed in 96-well plate and measured every 10 minutes until the plateau is reached in a Victor3 Plate reader (Perkin Elmer, USA) acquiring absorbance at 405 nm. P-nitrophenyl acetate (pNPA) and p-nitrophenol (pNP) (Sigma Aldrich, Germany) stock solutions were freshly prepared at 0.1 M in acetonitrile and diluted to desired final concentrations. The molar extinction coefficient was experimentally obtained from the calibration curve generated from a standard 4-nitrophenol (pNP) solution (Sigma Aldrich, United States), corresponding to 13014 M^{-1} cm^{-1} at 405 nm. Buffer signals was subtracted from all samples. Kinetic parameters were calculated using pNPA concentrations ranging from 0.2 to 1.5 mM. Reported results correspond to the average of at least three independent measurements. Kinetic parameters were obtained by fitting the data to the Michaelis-Menten equation [$V_0 = k_{cat} \cdot [E]_0 \cdot [S]_0 / (K_M + [S]_0)$] using GraphPad PRISM 5.0 software.

Chemical polymerization of pyrrole with HY-peptides. HY7, HY8, and HY9 peptides incubated at pH 8.0 were resuspended in 4 mM $CuCl_2$ in a 1.5 mL tube; additionally, 4 mM $CuCl_2$ was added to HY7, HY8 and HY9 peptides incubated at pH 4.0. 300 μL of freshly distilled pyrrole were added into a 20 mL vial and 1.5 mL tubes were carefully introduced in the corresponding vials, thus avoiding contact between both liquids to expose them to distilled pyrrole vapor. Reactions were incubated for 16 hours. As a reference, a solution of plain $CuCl_2$ with 250 or 750 µM L-Tyr was exposed to distilled pyrrole vapor. The resulting polymer was then resuspended, and the UV-vis spectra of the solutions were recorded. Pyrrole and L-Tyr were purchased from Sigma-Aldrich, Germany. $CuCl_2$ was purchased from Acros Organics, USA.

Electropolymerization of pyrrole with HY-peptides. Pyrrole and L-Tyr were purchased from Sigma-Aldrich. Na_2SO_4 was obtained from Panreac, USA. $CuCl_2$ was purchased from Acros Organics, USA. The electropolymerization of pyrrole was done by chronoamperometry in 0.1 M Na_2SO_4 at pH 8.0 and 4.0 using a lab-made three-electrode cell, with a platinum wire as a counter electrode, silver wire as a reference electrode, and an indium tin oxide (ITO) electrode as a working electrode. The potential applied to trigger the electropolymerization was 0.8 V vs Ag/AgCl. The concentration of pyrrole in the solution was 50 mM. The total volume of fibers solution was 1 mL. The sunken area of ITO electrode was 0.7 cm × 0.8 cm.

HY8 peptide hydrogel formation. 20 mM HY8 peptide stock solution was resuspended in 100 mM Tris HCl pH 8.0 in the presence of 50 μM of phenol red pH indicator to a final concentration of 5 mM. Since HFIP is acidic, the starting pH of the solution was around 4.0, remaining the peptide in a fluid state. The Eppendorf tube was led open overnight to allow HFIP evaporation and pH increased to 8.0, as determined by the change on color of phenol red from yellow to red/pink. HY8 peptide solution was then incubated at room temperature and quiescent conditions for 4 days. Hydrogel assembled at pH 8.0 was immediately disassembled by adding 200 μL of 100 mM Tris HCl 50 mM Citrate buffer at pH 4.0 with 50 μM phenol red.

HY8 peptide hydrogel catalytic activity. HY8 peptide hydrogel was assembled as described previously in a final volume of 200 μL, in this case, without phenol red pH indicator. To determine the catalytic activity, 20 μL of 1 mM pNPA solution were added into each sample and incubated at room temperature for 30 minutes. The acquisition of yellow coloration indicated the transformation of pNPA into pNP and thus esterase catalytic activity.

Molecular dynamics simulations. NPT Molecular dynamics simulations at 300 K were performed with the Amber suite, using the ff14SB force field.[48] To generate all possible parallel

fibrillar architectures of HY8d and H8Ye, we used an in-house code that computes the Cartesian coordinates of steric zippers of any length applying rigid rotations and translations to the coordinates of an individual strand. The length of each β-sheet was set to 20 strands, so that each fibril model is composed of 40 strands. For HY8d and H8Ye, we ran molecular dynamics simulations on the six non-equivalent parallel fibrillar architectures (**Figure S13**) and computed their relative energies on 100 frames sampled with a constant stride. See Supplementary Information for more details.

ASSOCIATED CONTENT

Supporting Information.

Computational methods.

Figure S1. Conformational characterization of HY-peptides incubated at pH 4.0 and pH 8.0.

Figure S2. Size characterization of the HY6, HY7, HY8, and HY9 assemblies at pH 8.0 by DLS.

Figure S3. Characterization of the amyloid-like properties for HY6 peptide incubated at pH 4.0 and pH 8.0.

Figure S4. Cell viability assay in the presence of HY7, HY8, and HY9 peptides.

Figure S5. TEM visualization of HY7, HY8 and HY9 peptides pH-dependent assembly, disassembly and reassembly.

Figure S6. HY8 assembly and disassembly cycles as a function of the pH.

Figure S7. QY7 assembly and disassembly as a function of the pH.

Figure S8. Lineweaver-Burk plots of pNPA hydrolysis catalyzed by 100 μM of HY7, HY8 and HY9 fibrils at pH 8.0.

Figure S9. Catalytic activity of HY7, HY8 and HY9 fibers at pH 7.4.

Figure S10. Lineweaver-Burk plots of pNPA hydrolysis catalyzed by 100 μM of HY7, HY8 and HY9 fibrils at pH 7.4.

Figure S11. Bioelectric and chemical polymerization of pyrrole by 750 uM L-Tyr at pH pH 8.0.

Figure S12. Bioelectric and chemical polymerization of pyrrole by L-Tyr, HY7, HY8 and HY9 peptides at pH 4.0.

Figure S13. Residue organization at the steric zipper of the 6 analyzed parallel fibril models.

Figure S14. HY8 δ-nitrogen protonated (HY8d) fibril models after 100 ns of molecular dynamics.

Figure S15. HY8 ε-nitrogen protonated (HY8e) fibril models after 100 ns of molecular dynamics.

Figure S16. Evolution of the β-sheet twist angles of the six HY8d steric zipper models.

Figure S17. Evolution of the β-sheet twist angles of the six HY8e steric zipper models.

Table S1. FTIR secondary structure assignments for HY6, HY7, HY8, and HY9 fibrils.

Table S2. pH transition values obtained from aggregation titter curves for HY7, HY8, and HY9 peptides.

Table S3. Kinetic parameters for HY7, HY8, and HY9 amyloid fibrils esterase activity at pH 8.0 and pH 7.4.

Table S4. Implicit solvent Amber energies (kcal/mol) and corresponding standard deviation of the twelve HY8 fibril models.

Table S5. Inter-sheet NCIIs of the twelve HY8 fibril models.

AUTHOR INFORMATION

Corresponding Author

***Salvador Ventura** - Institut de Biotecnologia i de Biomedicina and Departament de Bioquímica i Biologia Molecular; Universitat Autònoma de Barcelona; 08193 Bellaterra (Barcelona), Spain. Tel.: 34-93-5868956, Fax: 34-93-5811264, e-mail: salvador.ventura@uab.es

Author Contributions

Conceptualization, M.S., F.T., and S.V.; methodology, M. D.-C., M.N., F.P., L. R.-S. and S.N.; formal analysis and validation, M. D.-C., S.N. and S.V.; writing—review and editing, M. D.-C., S.N. and S.V.; supervision, S.N and S.V.; funding acquisition, S.V.

Funding Sources

This work was funded by the Spanish Ministry of Economy and Competitiveness BFU2013-44763-P and BIO2016-78310-R to S.V and by ICREA, ICREA-Academia 2015 to S.V. M. D.-C. was supported by the Spanish Ministry of Science and Innovation *via* a doctoral grant (FPU14/05786).

ACKNOWLEDGMENT

We acknowledge the technical support from the Cell Culture Unit of Servei de Cultius Cel·lulars i Producció d'Anticossos i Citometria (SCAC) and of the Servei de Microscopia from Universitat Autònoma de Barcelona (UAB). FP acknowledges the Mizutani Foundation for Glycoscience (200077). MS and LRS gratefully acknowledge financial support from MINECO (CTQ2017-89132-P) and the Generalitat de Catalunya (2017SGR1323).

NOTES

The authors confirm that there are no known conflicts of interest associated with this publication and there has been no significant financial support for this work that could have influenced its outcome.

REFERENCES

(1) Sorushanova, A.; Delgado, L. M.; Wu, Z.; Shologu, N.; Kshirsagar, A.; Raghunath, R.; Mullen, A. M.; Bayon, Y.; Pandit, A.; Raghunath, M.; Zeugolis, D. I. The Collagen Suprafamily: From Biosynthesis to Advanced Biomaterial Development. *Adv. Mater.* **2019**, *31* (1), 1–39.

(2) Falvo, M. R.; Gorkun, O. V.; Lord, S. T. The Molecular Origins of the Mechanical

Properties of Fibrin. *Biophys. Chem.* **2010**, *152* (1–3), 15–20.

(3) Askarieh, G.; Hedhammar, M.; Nordling, K.; Saenz, A.; Casals, C.; Rising, A.; Johansson, J.; Knight, S. D. Self-Assembly of Spider Silk Proteins Is Controlled by a PH-Sensitive Relay. *Nature* **2010**, *465* (7295), 236–238.

(4) Guerette, P. A.; Hoon, S.; Ding, D.; Amini, S.; Masic, A.; Ravi, V.; Venkatesh, B.; Weaver, J. C.; Miserez, A. Nanoconfined β-Sheets Mechanically Reinforce the Supra-Biomolecular Network of Robust Squid Sucker Ring Teeth. *ACS Nano* **2014**, *8* (7), 7170–7179.

(5) Wei, G.; Su, Z.; Reynolds, N. P.; Arosio, P.; Hamley, I. W.; Gazit, E.; Mezzenga, R. Self-Assembling Peptide and Protein Amyloids: From Structure to Tailored Function in Nanotechnology. *Chem. Soc. Rev.* **2017**, *46* (15), 4661–4708.

(6) Löwik, D. W. P. M.; Leunissen, E. H. P.; Van Den Heuvel, M.; Hansen, M. B.; Van Hest, J. C. M. Stimulus Responsive Peptide Based Materials. *Chem. Soc. Rev.* **2010**, *39* (9), 3394–3412.

(7) Jahn, T. R.; Makin, O. S.; Morris, K. L.; Marshall, K. E.; Tian, P.; Sikorski, P.; Serpell, L. C. The Common Architecture of Cross-β Amyloid. *J. Mol. Biol.* **2010**, *395* (4), 717–727.

(8) Otzen, D.; Riek, R. Functional Amyloids. *Cold Spring Harb. Perspect. Biol.* **2019**, *11* (12), 10.1101/cshperspect.a033860.

(9) Greenwald, J.; Kwiatkowski, W.; Riek, R. Peptide Amyloids in the Origin of Life. *J. Mol. Biol.* **2018**, *430* (20), 3735–3750.

(10) Nelson, R.; Eisenberg, D. Recent Atomic Models of Amyloid Fibril Structure. *Curr. Opin.*

Struct. Biol. **2006**, *16* (2), 260–265.

(11) Sawaya, M. R.; Sambashivan, S.; Nelson, R.; Ivanova, M. I.; Sievers, S. A.; Apostol, M. I.; Thompson, M. J.; Balbirnie, M.; Wiltzius, J. J. W.; McFarlane, H. T.; Madsen, A. Ø.; Riekel, C.; Eisenberg, D. Atomic Structures of Amyloid Cross-β Spines Reveal Varied Steric Zippers. *Nature* **2007**, *447* (7143), 453–457.

(12) Knowles, T. P. J.; Mezzenga, R. Amyloid Fibrils as Building Blocks for Natural and Artificial Functional Materials. *Adv. Mater.* **2016**, *28* (31), 6546–6561.

(13) Rufo, C. M.; Moroz, Y. S.; Moroz, O. V.; Stöhr, J.; Smith, T. A.; Hu, X.; Degrado, W. F.; Korendovych, I. V. Short Peptides Self-Assemble to Produce Catalytic Amyloids. *Nat. Chem.* **2014**, *6* (4), 303–309.

(14) Zhang, C.; Xue, X.; Luo, Q.; Li, Y.; Yang, K.; Zhuang, X.; Jiang, Y.; Zhang, J.; Liu, J.; Zou, G.; Liang, X. J. Self-Assembled Peptide Nanofibers Designed as Biological Enzymes for Catalyzing Ester Hydrolysis. *ACS Nano* **2014**, *8* (11), 11715–11723.

(15) Huang, Z.; Guan, S.; Wang, Y.; Shi, G.; Cao, L.; Gao, Y.; Dong, Z.; Xu, J.; Luo, Q.; Liu, J. Self-Assembly of Amphiphilic Peptides into Bio-Functionalized Nanotubes: A Novel Hydrolase Model. *J. Mater. Chem. B* **2013**, *1* (17), 2297–2304.

(16) Bal, S.; Das, K.; Ahmed, S.; Das, D. Chemically Fueled Dissipative Self-Assembly That Exploits Cooperative Catalysis. *Angew. Chemie* **2019**, *131* (1), 250–253.

(17) Makhlynets, O. V.; Korendovych, I. V. A Single Amino Acid Enzyme. *Nat. Catal. 2019 211* **2019**, *2* (11), 949–950.

(18) Al-Garawi, Z. S.; McIntosh, B. A.; Neill-Hall, D.; Hatimy, A. A.; Sweet, S. M.; Bagley, M. C.; Serpell, L. C. The Amyloid Architecture Provides a Scaffold for Enzyme-like Catalysts. *Nanoscale* **2017**, *9* (30), 10773–10783.

(19) Zhang, C.; Shafi, R.; Lampel, A.; MacPherson, D.; Pappas, C. G.; Narang, V.; Wang, T.; Maldarelli, C.; Ulijn, R. V. Switchable Hydrolase Based on Reversible Formation of Supramolecular Catalytic Site Using a Self-Assembling Peptide. *Angew. Chem. Int. Ed.* **2017**, *56* (46), 14511–14515.

(20) Jang, H.-S. S.; Lee, J.-H. H. J.; Park, Y.-S. S.; Kim, Y.-I. I. Y. Y.-O. O.; Park, J.; Yang, T.-Y. Y.; Jin, K.; Lee, J.-H. H. J.; Park, S.; You, J. M.; Jeong, K.-W. W.; Shin, A.; Oh, I.-S. S.; Kwon, M.-K. K.; Kim, Y.-I. I. Y. Y.-O. O.; Cho, H.-H. H.; Han, H. N.; Kim, Y.-I. I. Y. Y.-O. O.; Chang, Y.-H. H.; Paik, S. R.; Nam, K. T.; Lee, Y.-S. S. Tyrosine-Mediated Two-Dimensional Peptide Assembly and Its Role as a Bio-Inspired Catalytic Scaffold. *Nat. Commun.* **2014**, *5* (4), 1–11.

(21) Díaz-Caballero, M.; Navarro, S.; Fuentes, I.; Teixidor, F.; Ventura, S. Minimalist Prion-Inspired Polar Self-Assembling Peptides. *ACS Nano* **2018**, *12* (6), 5394–5407.

(22) Guo, H.; Zhang, J.; Xu, T.; Zhang, Z.; Yao, J.; Shao, Z. The Robust Hydrogel Hierarchically Assembled from a PH Sensitive Peptide Amphiphile Based on Silk Fibroin. *Biomacromolecules* **2013**, *14* (8), 2733–2738.

(23) Zhao, Y.; Yokoi, H.; Tanaka, M.; Kinoshita, T.; Tan, T. Self-Assembled PH-Responsive Hydrogels Composed of the RATEA16 Peptide. *Biomacromolecules* **2008**, *9* (6), 1511–1518.

(24) Watt, B.; Van Niel, G.; Raposo, G.; Marks, M. S. PMEL: A Pigment Cell-Specific Model for Functional Amyloid Formation. *Pigment Cell Melanoma Res*. **2013**, *26* (3), 300–315.

(25) Chuang, E.; Hori, A. M.; Hesketh, C. D.; Shorter, J. Amyloid Assembly and Disassembly. *J. Cell Sci*. **2018**, *131* (8), 1–18.

(26) Schneider, J. P.; Pochan, D. J.; Ozbas, B.; Rajagopal, K.; Pakstis, L.; Kretsinger, J. Responsive Hydrogels from the Intramolecular Folding and Self-Assembly of a Designed Peptide. *J. Am. Chem. Soc*. **2002**, *124* (50), 15030–15037.

(27) Aggeli, A.; Bell, M.; Carrick, L. M.; Fishwick, C. W. G.; Harding, R.; Mawer, P. J.; Radford, S. E.; Strong, A. E.; Boden, N. PH as a Trigger of Peptide β-Sheet Self-Assembly and Reversible Switching between Nematic and Isotropic Phases. *J. Am. Chem. Soc*. **2003**, *125* (32), 9619–9628.

(28) Ramachandran, S.; Flynn, P.; Tseng, Y.; Yu, Y. B. Electrostatically Controlled Hydrogelation of Oligopeptides and Protein Entrapment. *Chem. Mater*. **2005**, *17* (26), 6583–6588.

(29) Li, W.; Nicol, F.; Szoka, F. C. GALA: A Designed Synthetic PH-Responsive Amphipathic Peptide with Applications in Drug and Gene Delivery. *Adv. Drug Deliv. Rev*. **2004**, *56* (7), 967–985.

(30) Mondal, J.; Zhu, X.; Cui, Q.; Yethiraj, A. Sequence-Dependent PKa Shift Induced by Molecular Self-Assembly: Insights from Computer Simulation. *J. Phys. Chem. B* **2012**, *116* (1), 491–495.

(31) Hervas, R.; Rau, M. J.; Park, Y.; Zhang, W.; Murzin, A. G. A. G.; Fitzpatrick, J. A. J.;

Scheres, S. H. W.; Si, K. Cryo-EM Structure of a Neuronal Functional Amyloid Implicated in Memory Consolidation. *Science* **2020**, *367* (6483), 1230–1234.

(32) Ding, D.; Guerette, P. A.; Hoon, S.; Kong, K. W.; Cornvik, T.; Nilsson, M.; Kumar, A.; Lescar, J.; Miserez, A. Biomimetic Production of Silk-like Recombinant Squid Sucker Ring Teeth Proteins. *Biomacromolecules* **2014**, *15* (9), 3278–3289.

(33) Sun, Y.; Ding, F. Thermo- and PH-Responsive Fibrillization of Squid Suckerin A1H1 Peptide. *Nanoscale* **2020**, *12* (11), 6307–6317.

(34) Woody, R. W. Aromatic Side-chain Contributions to the Far Ultraviolet Circular Dichroism of Peptides and Proteins. *Biopolymers* **1978**, *17* (6), 1451–1467.

(35) Serpell, L. C. Alzheimer's Amyloid Fibrils: Structure and Assembly. *Biochim. Biophys. Acta - Mol. Basis Dis.* **2000**, *1502* (1), 16–30.

(36) Marina, G. B.; Kirkitadze, D.; Lomakin, A.; Vollers, S. S.; Benedek, G. B.; Teplow, D. B. Amyloid β-Protein (Aβ) Assembly: Aβ40 and Aβ42 Oligomerize through Distinct Pathways. *Proc. Natl. Acad. Sci. U. S. A.* **2003**, *100* (1), 330–335.

(37) Sant'anna, R.; Navarro, S.; Ventura, S.; Paraoan, L.; Foguel, D. Amyloid Properties of the Leader Peptide of Variant B Cystatin C: Implications for Alzheimer and Macular Degeneration. *FEBS Lett.* **2016**, *590* (5), 644–654.

(38) Díaz-Caballero, M.; Navarro, S.; Ventura, S. Soluble Assemblies in the Fibrillation Pathway of Prion-Inspired Artificial Functional Amyloids Are Highly Cytotoxic. *Biomacromolecules* **2020**, *21* (6), 2334–2345.

(39) Armstrong, K. M.; Baldwin, R. L. Charged Histidine Affects α-Helix Stability at All Positions in the Helix by Interacting with the Backbone Charges. *Proc. Natl. Acad. Sci. U. S. A.* **1993**, *90* (23), 11337–11340.

(40) Godzhaev, N. M. Study of Trypsin-Substrate and Trypsin-Inhibitor Complexes. 1. Conformation of Asp-102, His-57 and Ser-195 Residues in the Trypsin Active Center. *Mol. Biol.* **1984**, *18* (5), 1432–1435.

(41) Gutfreund, H.; Sturtevant, J. M. The Mechanism of the Reaction of Chymotrypsin with P-Nitrophenyl. *Biochem. J.* **1956**, *63* (4), 656–661.

(42) Maeda, Y.; Makhlynets, O. V.; Matsui, H.; Korendovych, I. V. Design of Catalytic Peptides and Proteins Through Rational and Combinatorial Approaches. *Annual Review of Biomedical Engineering*. Annual Reviews Inc. July 11, 2016, pp 311–328.

(43) Ishikita, H.; Knapp, E. W. Function of Redox-Active Tyrosine in Photosystem II. *Biophys. J.* **2006**, *90* (11), 3886–3896.

(44) Kim, S.; Cho, H. J.; Lee, N.; Lee, Y. S.; Shin, D. S.; Lee, S. M. A Phase-Reversible Pd Containing Sphere-to-Bridge-Shaped Peptide Nanostructure for Cross-Coupling Reactions. *RSC Adv.* **2017**, *7* (53), 33162–33165.

(45) Asavapiriyanont, S.; Chandler, G. K.; Gunawardena, G. A.; Pletcher, D. The Electrodeposition of Polypyrrole Films from Aqueous Solutions. *J. Electroanal. Chem.* **1984**, *177* (1–2), 229–244.

(46) Peccati, F. NCIPLOT4 Guide for Biomolecules: An Analysis Tool for Noncovalent Interactions. *J. Chem. Inf. Model.* **2020**, *60* (1), 6–10.

(47) Miller, Y.; Ma, B.; Nussinov, R. Polymorphism in Self-Assembly of Peptide-Based β-Hairpin Contributes to Network Morphology and Hydrogel Mechanical Rigidity. *J. Phys. Chem. B* **2015**, *119* (2), 482–490.

(48) Maier, J. A.; Martinez, C.; Kasavajhala, K.; Wickstrom, L.; Hauser, K. E.; Simmerling, C. Ff14SB: Improving the Accuracy of Protein Side Chain and Backbone Parameters from Ff99SB. *J. Chem. Theory Comput.* **2015**, *11* (8), 3696–3713.

Table of Contents

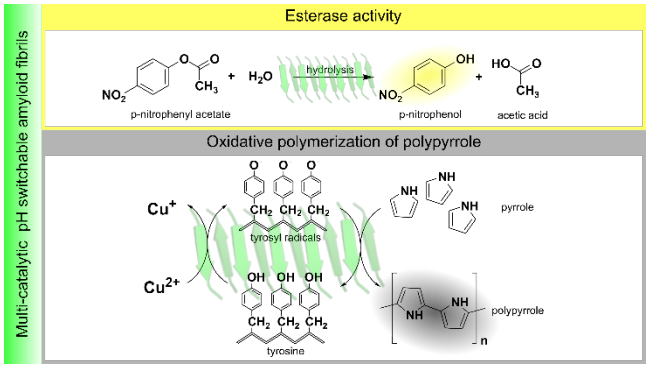

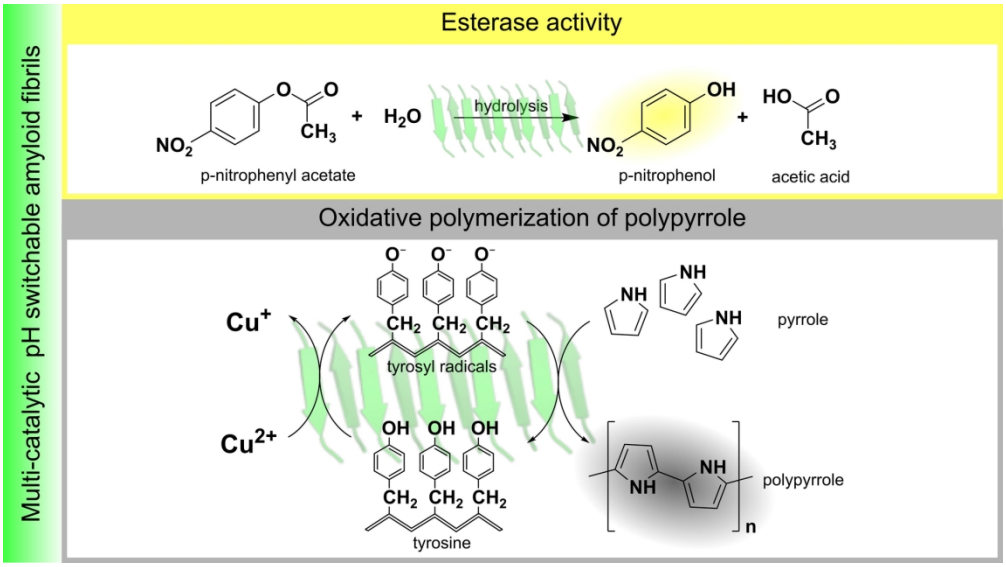

Table of contents

85x47mm (600 x 600 DPI)